INTERNATIONAL JOURNAL FOR NUMERICAL METHODS IN FLUIDS, VOL. 15, 377–397 (1992)

FLOW CHARACTERISTICS IN THE DOWNSTREAM REGION OF A CONICAL DIFFUSER

P. PRINOS AND A. GOULAS

Laboratory of Fluid Mechanics and Turbomachinery, Department of Mechanical Engineering, University of Thessaloniki, 540 06 Thessaloniki, Greece

SUMMARY

Using the Navier–Stokes equations in conjunction with the k–ε model of turbulence, the characteristics of flow in the region downstream of a conical diffuser with 5° angle of inclination are calculated. Two representative stations $1D_2$ and $10D_2$ after the diffuser exit are selected for comparison against experimental results. The calculations indicate an underestimation of mean velocity and turbulence kinetic energy at the first station, while satisfactory agreement is obtained for the mean velocity at the second station. The use of a modified k–ε model sensitive to adverse pressure conditions improves the predictions considerably. The effect of inlet properties and Reynolds number on the flow characteristics at the above stations is studied using various inlet profiles and a range of Reynolds numbers based on the inlet diameter from 50 000 to 280 000.

KEY WORDS Diffuser k–ε model General co-ordinates Momentum interpolation Adverse pressure

1. INTRODUCTION

Flow through axisymmetric diffusers is encountered in many engineering applications and its accurate prediction is essential. In general, axisymmetric diffusers can be divided into (i) those with small total angle (5°–10°) where the flow remains attached for the whole length and (ii) those with large total angle and significant separation of flow within the diffuser. For the latter, experiments have been conducted by several investigators, e.g. Chaturvedi,[1] Weiser and Nitsche[2] and Stieglmeier *et al.*,[3] and calculations have been performed by Habib and Whitelaw[4] and Armfield and Fletcher.[5] Diffusers with small total angle have been examined by Waitman *et al.*,[6] Kline *et al.*,[7] Livesey and Turner,[8] Bradley and Cockrell,[9] Fraser,[10] Nakamura *et al.*[11] and Okwuobi and Azad[12] among others. Recently Azad and Kassab[13] examined experimentally the turbulent flow in a conical diffuser with 8° total angle and pointed out the complexity of the flow.

In most of the above studies the emphasis was on the effect of the inlet profile on the performance of the diffusers and also on the flow characteristics within the diffuser. Armfield and Fletcher[5] also performed some calculations and comparisons against Fraser's[10] experimenal results using an algebraic eddy viscosity turbulence model.

In this study attention is restricted to the flow characteristics in the downstream region and to the predictive ability of the k–ε model of turbulence in this region. A finite volume method is used for the solution of the Navier–Stokes equations together with the k–ε model of turbulence in a conical diffuser with half-angle approximately 5° and diameter ratio $D_2/D_1 = 2{\cdot}0$.

The equations were initially solved using cylindrical co-ordinates with a stepwise approximation for the inclined boundary. Subsequently the equations were solved using general non-

0271–2091/92/160377–21$15.50

Received March 1991
Revised January 1992

orthogonal boundary-fitted co-ordinates and hence the approximations introduced by the first approach could be studied. A comparison of characteristic results produced by both techniques is given in Section 4. Detailed computed results using cylindrical co-ordinates are given elsewhere.[14]

Two stations in the region downstream of the diffuser[15] are selected for comparison since experimental measurements are available. The first station is located $1D_2$ after the diffuser exit where the velocity profile is highly non-uniform and adverse pressure conditions still influence the flow characteristics. The second station is located $10D_2$ after the diffuser exit where the flow starts to redevelop and has a quite 'flat' velocity profile. The total length of the downstream pipe was $15D_2$. A short description of the experimental procedure and measurements is given in Section 3.

The effect of the turbulence model on the prediction of flow at the above stations was studied by using also a modified version of the k–ε model accounting for the adverse pressure conditions existing at the first station. The model has been applied by several investigators, e.g. Rodi and Scheuerer,[16] Hanjalic and Launder,[17] De Henau *et al.*[18] and Nagano and Tagawa,[19] in adverse pressure gradient boundary layers and has been found to yield improved predictions for moderate adverse pressure gradients.

In this model the dissipation equation is sensitized to irrotational strains by multiplying the irrotational contribution to the production of turbulent kinetic energy by a higher constant than that used to multiply the rotational part.

Finally, the effect of inlet properties and Reynolds number ($Re = U_m D_1/v$) on the flow characteristics in the above stations is studied numerically using three different inlet profiles (experimental, fully developed and uniform) for three different Reynolds numbers ranging from 50 000 to 280 000.

It should be mentioned that the computational study was conducted independently from the experimental study and hence the techniques and models used can be considered as 'pure' predictive tools.

2. COMPUTATIONAL PROCEDURE

In this section the governing equations for steady, turbulent, two-dimensional incompressible flow are presented in cylindrical co-ordinates together with the standard and modified k–ε models of turbulence. The methodology for transforming the equations in general non-orthogonal boundary-fitted co-ordinates is presented next. Finally, the computational method for solving the set of algebraic equations is presented together with the appropriate boundary conditions.

2.1. Governing equations

For steady, turbulent, two-dimensional incompressible flow the Navier–Stokes equations, based on the eddy viscosity concept, in cylindrical co-ordinates take the following form:

continuity equation

$$\frac{\partial U}{\partial x}+\frac{1}{r}\frac{\partial r V}{\partial r}=0, \tag{1}$$

x-momentum equation

$$\frac{\partial}{\partial x}(\rho U^2)+\frac{1}{r}\frac{\partial}{\partial r}(\rho r V U)=-\frac{\partial p}{\partial x}+2\frac{\partial}{\partial x}\left(\mu_{\text{eff}}\frac{\partial U}{\partial x}\right)+\frac{1}{r}\frac{\partial}{\partial r}\left(\mu_{\text{eff}} r\frac{\partial U}{\partial r}\right)+\frac{1}{r}\frac{\partial}{\partial r}\left(\mu_{\text{eff}} r\frac{\partial V}{\partial x}\right), \tag{2}$$

r-momentum equation

$$\frac{\partial}{\partial x}(\rho U V)+\frac{1}{r}\frac{\partial}{\partial r}(\rho r V^2)=-\frac{\partial p}{\partial r}+2\frac{1}{r}\frac{\partial}{\partial r}\left(\mu_{\text{eff}} r\frac{\partial V}{\partial r}\right)+\frac{\partial}{\partial x}\left(\mu_{\text{eff}}\frac{\partial V}{\partial x}\right)+\frac{\partial}{\partial x}\left(\mu_{\text{eff}}\frac{\partial U}{\partial x}\right)-2\mu_{\text{eff}}\frac{V}{r^2}, \tag{3}$$

where U and V are the velocity components in the x- and r-directions respectively, p is the local effective mean pressure, μ_{eff} is the effective viscosity and ϱ is the density of fluid.

The effective viscosity μ_{eff} contains both the laminar and turbulent viscosities (μ_e and μ_t respectively). The latter is calculated from the k–ε model of turbulence via the relationship

$$\mu_t=\rho c_\mu k^2/\varepsilon, \tag{4}$$

where k is the turbulent kinetic energy, ε is the rate of dissipation and c_μ is a constant (0·09).

The transport equations for k and ε used in the k–ε model are described as follows:

transport of k

$$\frac{\partial}{\partial x}(\rho U k)+\frac{1}{r}\frac{\partial}{\partial r}(\rho r V k)=\frac{\partial}{\partial x}\left(\frac{\mu_{\text{eff}}}{\sigma_k}\frac{\partial k}{\partial x}\right)+\frac{1}{r}\frac{\partial}{\partial r}\left(\frac{\mu_{\text{eff}}}{\sigma_k} r\frac{\partial k}{\partial r}\right)+P_k-\rho\varepsilon, \tag{5}$$

transport of ε

$$\frac{\partial}{\partial x}(\rho U\varepsilon)+\frac{1}{r}\frac{\partial}{\partial r}(\rho r V\varepsilon)=\frac{\partial}{\partial x}\left(\frac{\mu_{\text{eff}}}{\sigma_\varepsilon}\frac{\partial \varepsilon}{\partial x}\right)+\frac{1}{r}\frac{\partial}{\partial r}\left(\frac{\mu_{\text{eff}}}{\sigma_\varepsilon} r\frac{\partial \varepsilon}{\partial r}\right)+c_1\frac{\varepsilon}{K}P_k-c_2\rho\frac{\varepsilon^2}{k}, \tag{6}$$

where σ_k, σ_ε, σ_1, c_2 are constants (1·0, 1·3, 1·44 and 1·92 respectively) and P_k is the production of turbulent kinetic energy. The values of the above constants are the standard ones suggested by Launder and Spalding.[20]

The production term P_k is analysed as

$$P_k=-\overline{u^2}\frac{\partial U}{\partial x}-\overline{v^2}\frac{1}{r}\frac{\partial r V}{\partial r}-\overline{uv}\left(\frac{\partial U}{\partial r}+\frac{\partial V}{\partial x}\right), \tag{7}$$

where $\overline{u^2}$ and $\overline{v^2}$ are the normal stresses in the x- and r- directions respectively and uv is the shear stress. Applying also the Boussinesq approximation to the stresses appearing in (7), the production term used in the k–ε model has the form

$$P_k=\mu_{\text{eff}}\left\{2\left[\left(\frac{\partial U}{\partial x}\right)^2+\left(\frac{\partial V}{\partial r}\right)^2+\left(\frac{V}{r}\right)^2\right]+\left(\frac{\partial U}{\partial r}+\frac{\partial V}{\partial x}\right)^2\right\}. \tag{8}$$

Hanjalic and Launder[17] have used the production term P_k in the ε-equation in a modified way by sensitizing the irrotational part of P_k. They did this by multiplying the first two terms of (7) by an empirical coefficient c_3 larger than the c_1 used to multiply the third term. Hence the term $c_1(\varepsilon/k)P_k$ in the ε-equation takes the form

$$c_1\frac{\varepsilon}{k}P_k=\frac{\varepsilon}{k}\left[-c_1\overline{uv}\left(\frac{\partial U}{\partial r}+\frac{\partial V}{\partial x}\right)-c_3(\overline{u^2}-\overline{v^2})\frac{\partial U}{\partial x}\right]. \tag{9}$$

A value of c_3 of 4·44 has been recommended by Hanjalic and Launder.[17] Rodi and Scheuerer[16] have used 2·5 for high-adverse-pressure-gradient flows, while De Henau *et al.*,[18] have used values

from 2·5 to 5·50 to determine the sensitivity of a turbulent separating boundary layer flow to c_3. In general this modification gives rise to larger ε-values and the model becomes more sensitive to deceleration. Two values of c_3 have been used in the present study (2·5 and 4·44) to check the sensitivity of computations to c_3.

Hanjalic and Launder[17] have also used the following expression for the normal stresses:

$$\overline{u^2}-\overline{v^2}=0{\cdot}33\,k, \tag{10}$$

in which the value of 0·33 is in agreement with experimental results for boundary layers with adverse pressure gradients. The same expression has been used in the present study. However, a more refined approach can be used in which $\overline{u^2}$ and $\overline{v^2}$ are calculated directly from an algebraic stress model. Such an approach has been followed by Nagano and Tagawa[19] in conjunction with a low-Reynolds-number k–ε model for predicting a variety of flows.

Using the calculation procedure described in Reference 21, the above equations (1)–(3), (5) and (6) can be put in a common form as

$$\frac{\partial}{\partial x}(\rho U\phi)+\frac{1}{r}\frac{\partial}{\partial r}(\rho r V\phi)=S_\phi+\frac{\partial}{\partial x}\left(\Gamma_\phi\frac{\partial\phi}{\partial x}\right)+\frac{1}{r}\frac{\partial}{\partial r}\left(\Gamma_\phi r\frac{\partial\phi}{\partial r}\right), \tag{11}$$

where Γ_ϕ is the effective diffusion coefficient, S_ϕ is a source term and $\phi=1$ (continuity equation), U, V (momentum equations), k and ε(k–ε transport equations).

2.2. *Transformation of governing equations*

Using a boundary-fitted non-orthogonal grid as shown in Figure 1, the governing equations in cylindrical co-ordinates must be transformed to general non-orthogonal co-ordinates.

The first step is to transform the flow area in the real (x, y)-plane into a parallelogram in a (ξ, n)-plane according to the general transformation $\xi=\xi(x, y)$ and $n=n(x, y)$. The transformation is generated following the procedure of Thompson *et al.*,[22] who solve two elliptic equations with appropriate boundary conditions.

The second step is to transform equation (11) in the (ξ, n)-plane but maintaining the same dependent variables. Another methodology can also be followed by writing the equation directly, using velocity components normal to ξ- and n-lines as dependent variables, but the equations are complex.[23] Hence equation (11) takes the desired conservative form

$$\frac{\partial}{\partial\xi}(rU_1\phi)+\frac{\partial}{\partial n}(rV_1\phi)=\frac{\partial}{\partial\xi}\left(rC_1\frac{\partial\phi}{\partial\xi}+rC_2\frac{\partial\phi}{\partial n}\right)+\frac{\partial}{\partial n}\left(rC_3\frac{\partial\phi}{\partial n}+rC_4\frac{\partial\phi}{\partial\xi}\right)+JS_\phi, \tag{12}$$

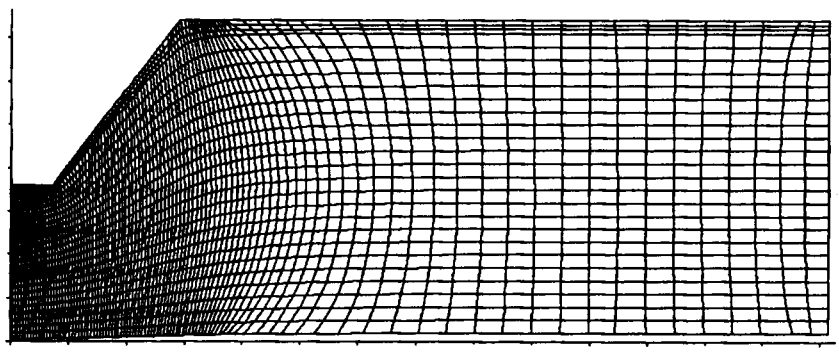

Figure 1. Typical non-orthogonal grid used in the study

where U_1 and V_1 are contravariant velocity components related to U and V by $U_1 = y_n U - x_n V$ and $V_1 = x_\xi U - y_\xi V$ respectively and C_1, C_2, C_3 and C_4 are coefficients given by

$$C_1 = \frac{\Gamma_\phi \alpha}{J}, \qquad C_2 = C_4 = -\frac{\Gamma_\phi \beta}{J}, \qquad C_3 = \frac{\Gamma_\phi \gamma}{J}, \tag{13}$$

in which J is the Jacobian of the transformation between a given physical plane and the corresponding transformed plane ($J = x_\xi y_n - x_m^n y_\xi$), and $\alpha = x_n^2 + y_n^2$, $\beta = x_\xi x_\eta + y_\xi y_n$ and $\gamma = x_\xi^2 + y_\xi^2$.

In equation (12) partial derivatives of ϕ and of any function have been transformed according to

$$\phi_x = \frac{y_n \phi_\xi - y_\xi \phi_n}{J}, \qquad \phi_y = \frac{x_n \phi_\xi + x_\xi \phi_n}{J}. \tag{14}$$

2.3. Computational method

For a typical node P enclosed in its cell and surrounded by its neighbours N, S, E and W as shown in Figure 2, equation (11) can be transformed using Patankar's procedure into a relationship between ϕ_p and the neighbouring values as follows:

$$A_P \phi_P = A_E \phi_E + A_W \phi_W + A_N \phi_N + A_S \phi_S + S_\phi J \Delta V - [(rC_2 \phi_n \Delta n)_w \xi + (rC_4 \phi_\xi \Delta \xi)_s n], \tag{15}$$

where the coefficients A involve the flow properties of convection, diffusion, etc. and are modified according to a 'hybrid scheme' which evaluates the convective terms by the first-order upwind-differencing scheme whenever the grid cell Peclet number is greater than 2.

The terms within the square brackets in equation (15) originate from the cross-derivatives in the diffusion terms and are a result of the non-orthogonal co-ordinate system. They are usually small and can be combined with the source term and treated as known quantities.

The velocities obtained from equation (15) should also satisfy the continuity equation. The latter is transformed into a Poisson equation and the concept of 'pressure correction' is used as in

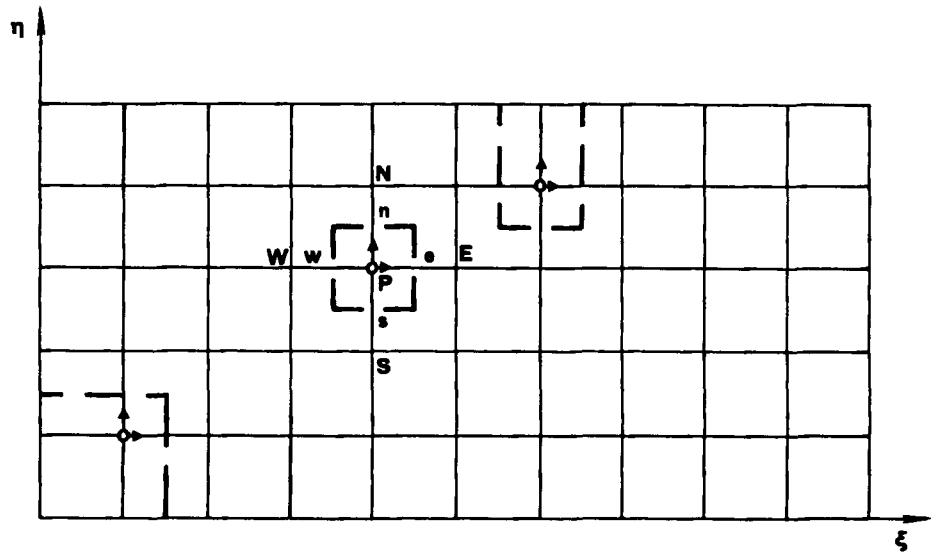

Figure 2. Computational plane and typical control volume with non-staggered arrangement of variables

the SIMPLE algorithm of Patankar. Difficulties arise owing to the non-staggered arrangement of variables (Figure 2) if linear interpolation for the evaluation of the mass fluxes at the cell faces is used. Rhie and Chow[24] reported pressure oscillations and proposed a different interpolation scheme to overcome the problem (momentum interpolation).

Similar practice is used in this study for the evaluation of the velocity component at a cell face. The discretized momentum equations for the two neighbouring control volumes around the face are used for the interpolation, where the pressure gradient term is not interpolated but is replaced by the difference in pressure at the cell centres between which the cell face lies. Peric[25] and Majumdar[26] have also used this interpolation formula quite successfully for cell face velocities in conjunction with the SIMPLE algorithm for the prediction of complex flows.

Hence, for example, the velocity U_e needed for the calculation of the mass flux at the e-face is calculated from the expression

$$U_e=\tfrac{1}{2}(H_{i,j}+H_{i+1,j})+\tfrac{1}{2}\left(\frac{1}{A_{pi,j}}+\frac{1}{A_{pi+1,j}}\right)D_{1,ij}(P_{i,j}-P_{i+1,j}), \tag{16}$$

where

$$H_{i,j}=\frac{A_E U_{i+1,j}+A_w U_{i-1,j}+A_N U_{i,j+1}+A_S U_{i,j-1}+S_U \Delta V}{A_{pi,j}}+D_{2,ij}(P_{i,j+1}-P_{i,j})$$

and $D_{1,ij}$ and $D_{2,ij}$ are coefficients of the pressure terms.

Finally, a line-by-line relaxation technique is employed in the solution of the algebraic equations, using the TDMA (tridiagonal matrix algorithm) for the update of a variable at all points along a column.

2.4. *Boundary conditions*

The following boundary conditions have been applied in the present study.

Inlet. Three different profiles for all the dependent variables were used as inlet conditions at a station $2D_1$ upstream of the diffuser entrance. At this station experimental results were available[15] for the mean velocity U and the stresses $\overline{u^2}$, $\overline{v^2}$ and $\overline{uv}$. Hence the turbulent kinetic energy k was calculated from the above normal stresses assuming that $\overline{v^2}=\overline{w^2}$, while the ε-profile, assuming local equilibrium, was obtained through the relationship $\varepsilon=-\overline{uv}\,\partial U/\partial y$. At the above station measurements indicated that the flow was nearly fully developed.

Also, fully developed profiles of U, k and ε were used as inlet conditions after running the programme for a sufficient length of time in a pipe of diameter D_1.

The difference between experimental and computational inlet profiles is shown in Figure 3 together with the uniform profiles used as a third choice.

Hence the effect of the inlet profile on the flow characteristics downstream of a diffuser could be studied.

Outlet. The outlet station was placed at a distance of 2·832 m from the inlet station or alternatively $15D_2$ downstream of the diffuser exit. At this station values of the dependent variables were evaluated by quadratic extrapolation from upstream neighbours. In the case of velocity, however, the convective fluxes were corrected to satisfy overall continuity.

Symmetry axis. On a symmetry axis the conditions which have to be satisfied are (i) no cross-flow, (ii) zero diffusion flux of the variable in a direction normal to the symmetry axis and (iii) the cross-derivative diffusion terms across the symmetry axis, which are included in the source term, should be zero.

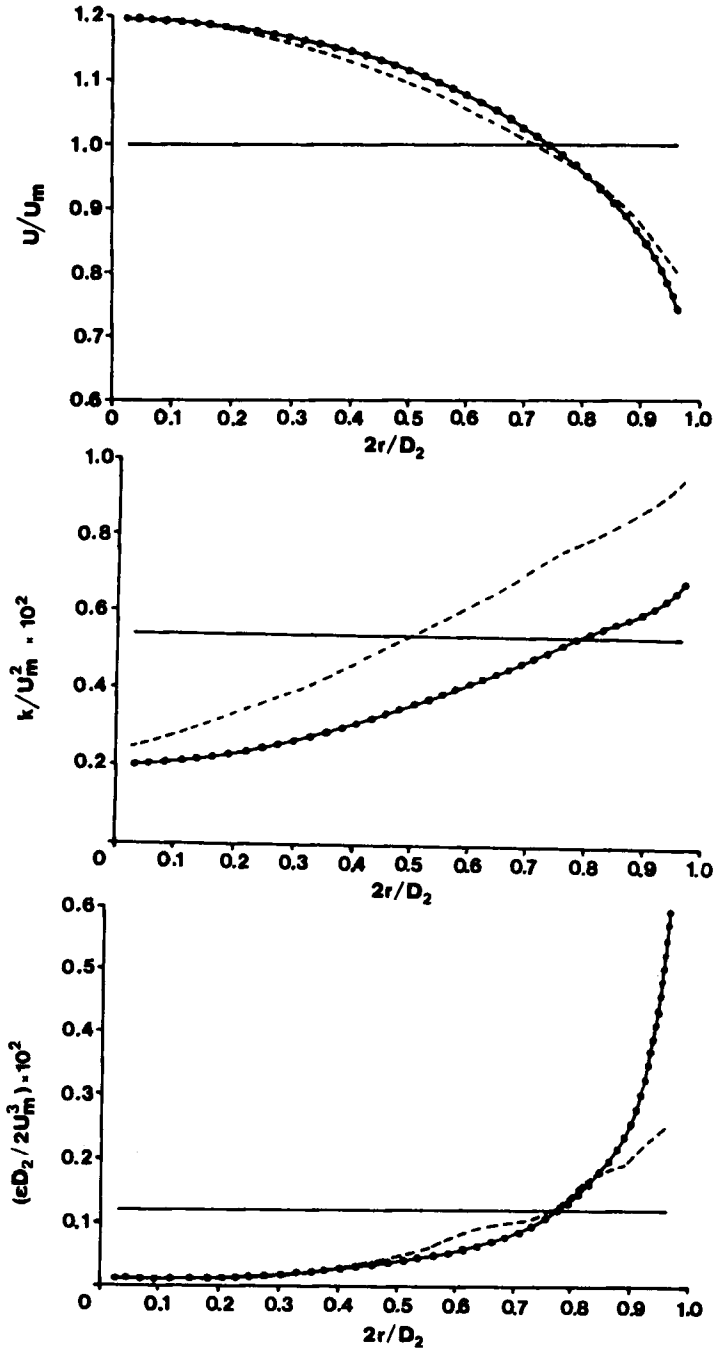

Figure 3. Inlet profiles for (a) velocity, (b) turbulent kinetic energy and (c) rate of dissipation: – – – –, experiments; ——, uniform; –●–●–●, fully developed

The values of any dependent variable ϕ on the symmetry axis are updated according to $\partial\phi/\partial n = 0$ and the value of ϕ on the symmetry axis is evaluated by extrapolation from the interior values.

Wall. For the calculation of the velocity at the first grid point near a wall the wall function approach of Launder and Spalding[20] is followed whereby the wall shear stress vector is expressed as a function of the adjacent velocity component parallel to the wall. In the general co-ordinate system used here the wall shear stress affects the momentum conservation in both directions (Figure 4).

The wall shear stress vector is written as

$$\tau_w = -\lambda_w \mathbf{U}_p \tag{17}$$

where λ_w is expressed from a 'universal velocity profile'. For the laminar sublayer ($y_{p+} < 11{\cdot}6$) λ_w is given as $\lambda_w = \mu/\Delta n$, while for the fully turbulent layer

$$\lambda_w = -\frac{\rho c_\mu^{1/4} k^{1/2} \kappa}{\ln(E y_p^+)}, \tag{18}$$

where κ is the von Karman constant (0·4187), E is the roughness parameter (9·793) and y_{p+} is calculated as

$$y_p^+ = \frac{\rho c_\mu^{1/4} k_p^{1/2} \Delta n}{\mu}. \tag{19}$$

The shear force T_w acting along U_p is decomposed into two components T_{w2} and T_{w2} along U and V respectively, which are used in the momentum equations as follows:

$$T_{w1} = -\lambda_w A_w[(1-n_1^2)U - n_1 n_2 V], \qquad T_{w2} = -\lambda_w A_w[(1-n_2^2)V - n_1 n_2 U], \tag{20}$$

where n_1 and n_2 are the components of the unit vector along x and y respectively (outward normal to the wall) and A_w is the length of the control volume face at the wall (Figure 4).

The equations for k and ε also require special treatment near the wall. In the equation for k the diffusion flux through the wall face is set to zero and the generation of k is calculated separately from a formula based on the law of the wall:

$$P_k = \frac{|\tau_w|\,|\mathbf{U}_p|}{\Delta n}. \tag{21}$$

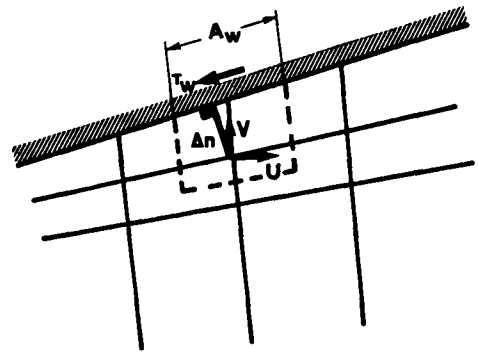

Figure 4. Typical wall boundary

In the equation for ε the value of ε near the wall is calculated from the local value of k using the concept of equilibrium between production and dissipation of k:

$$\varepsilon = \frac{c_\mu^{3/4} k^{3/2}}{\kappa \Delta n}. \tag{22}$$

3. EXPERIMENTAL PROCEDURE AND MEASUREMENTS

The main flow section of the flow circuit used in the experimental programme is shown in Figure 5. It consisted of an upstream pipe 4·0 m long and of diameter 74 m followed by the diffuser section 0·434 m long and the downstream pipe 1·0 m long and of diameter 150 mm. The above section was connected to a 35 kW centrifugal fan with nominal characteristics of 1600 Pa pressure rise at 5 $m^3 s^{-1}$ flow rate. The latter was measured with a turbine flowmeter located at the downstream end of the flow section. A comparison of the turbine meter indications with the calculated flow rate from velocity measurements indicated a difference of up to 3%.

Measurements were performed using a laser Doppler anemometer (LDA) and a hot-wire anemometer (H-W) for comparison purposes.

The former was a DANTEC forward scatter system measuring one component and consisting of a Hughes 15 mW laser tube, forward scatter optics, a Bragg cell section, a photomultiplier and a counter. The analogue signal from the counter was sent to an IBM PC/XT computer through a 12 bit A/D converter capable of sampling at frequencies up to 20 kHz.

The H-W measurements were performed with a cross-type DANTEC 55P61 probe connected to a DANTEC 55M01 unit with a standard bridge, two digital voltmeters and two DANTEC 55M35 RMS units. The signal was filtered and the AC was input to the computer. Using the above probe, time-mean velocities in the horizontal and radial directions, turbulence intensities u' and v' and shear stress $\overline{uv}$ were measured at the inlet station and the two downstream stations.

A comparison between LDA and H-W measurements indicated a maximum difference of 3%. A detailed description of the experimental procedure and measurements is given elsewhere.[15]

4. COMPUTATIONAL AND EXPERIMENTAL RESULTS

The computational results presented in this section are based on general non-orthogonal boundary-fitted co-ordinates. However, cylindrical co-ordinates were also applied with a step-wise approximation for the diffuser wall. A comparison of selected flow characteristics based on the above two techniques is described below.

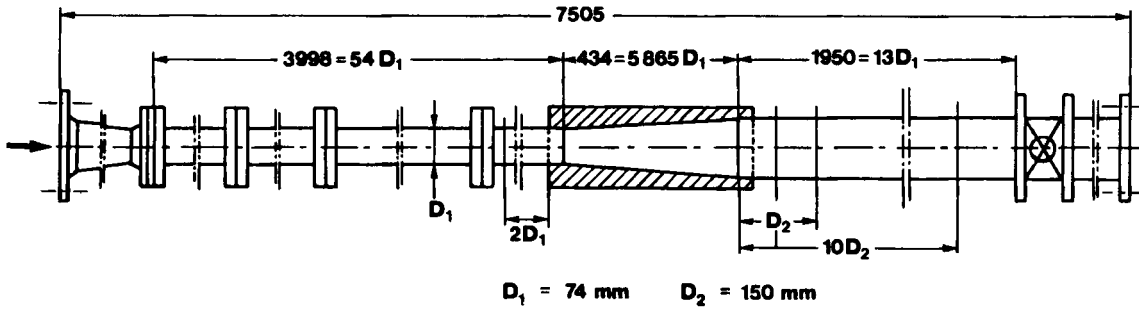

Figure 5. Main flow section

Figure 6 shows the predicted c_p-distribution along the symmetry axis of flow using cylindrical co-ordinates with a stepwise approximation of the diffuser wall and boundary-fitted general co-ordinates. The steps used in the first approach (approximately 10 steps with three to five vertical lines per step) reduce c_p in the downstream section, although the pressure gradient is almost the same for both cases.

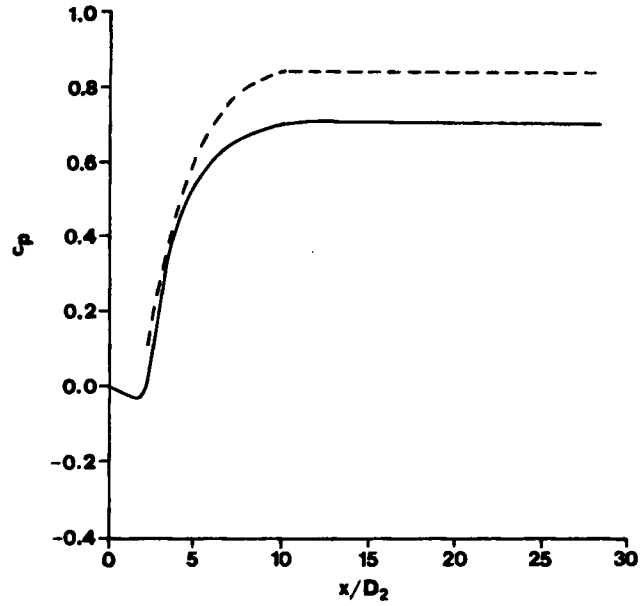

Figure 6. Calculation of c_p along flow section: ——, cylindrical; – – – –, non-orthogonal

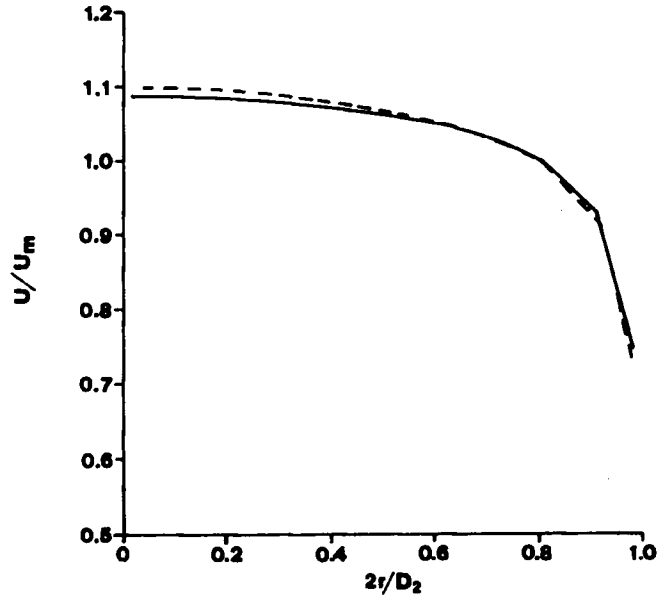

Figure 7. Comparison of computed velocities by both techniques at second station: ——, cylindrical; – – – –, non-orthogonal

Figure 7 shows the predicted velocity distribution at the second station using both techniques. Minor differences are observed, especially near the wall. Similar trends are observed for the turbulence characteristics. In general, great care is required when the stepwise approximation is used, especially for low angles of inclination.

Before studying the effect of the turbulence model, Reynolds number and inlet properties on the flow characteristics at the two downstream stations of the diffuser, grid independence checks were performed which are described below.

4.1. Grid independence checks

Initially a non-uniform grid consisting of 80×30 grid nodes was used (80 and 30 grid lines in the longitudinal and vertical directions respectively) and subsequently it was doubled (160×60) in order to check the dependence of the results on the grid used. Figures 8 and 9 show the difference in flow characteristics at the two stations downstream of the diffuser. Significant differences are observed at the first station downstream of the diffuser where the velocity profile is quite sharp, especially for the turbulent kinetic energy (Figures 8(b) and 9(b)). A further refinement of the grid (200×80) produced only minor differences. Hence the 160×60 grid was used for all subsequent calculations, which also required less computational time than the finest grid.

4.2. Effect of turbulence model

The effect of the turbulence model was studied by applying the standard and modified k–ε models of turbulence as described before, for a Reynolds number ($Re = D_1 U_{mean}/v$) equal to 105 000, for which experimental measurements at both stations were taken. The initial profiles for U, k and ε used in this case are the experimental profiles shown in Figures 3(a)–3(c) respectively.

Figures 10(a)–10(c) show the experimental and predicted profiles of velocity, turbulent kinetic energy and its rate of dissipation respectively at the first downstream station. The experimental k-profile is derived from measurements of $\overline{u^2}$ and $\overline{v^2}$. Assuming that $\overline{v^2} = \overline{w^2}$, the values of k have been calculated from $k = \frac{1}{2}(\overline{u^2} + 2\overline{v^2})$. Owing to the adverse pressure gradient conditions existing in the region, the standard k–ε model is found to significantly underpredict the velocity in the core flow, while the modified k–ε model, sensitive to such conditions, is found to agree satisfactorily with the experimental profile. When using the value $c_3 = 2{\cdot}5$ instead of the classical 4·44 used in other studies,[16,17] the velocity profile is calculated to be between those predicted by the standard and modified models. This indicates the sensitivity of the modified model to the choice of the empirical constant c_3.

Figure 10(b) compares predicted and experimental k-profiles at the same station. The standard k–ε model overpredicts the kinetic energy near the symmetry axis and underpredicts it near the wall, while the modified model ($c_3 = 4{\cdot}44$) shows better behaviour near the symmetry axis and similar predictions near the wall.

Figures 11(a)–11(c) show the respective profiles at the second downstream station. At this station the adverse pressure gradient conditions no longer exist; the flow has lost its 'diffusive' character and starts to redevelop. Hence both models give similar predictions which are in satisfactory agreement with the experimental velocity profile. However, predicted and experimental values of k (Figure 11(b)) are in total disagreement near the wall, since predictions in this region are smaller than those near the symmetry axis. Experimental values are higher near the wall, indicating the 'boundary layer' type of flow which starts to develop in this region. The anisotropy of flow, observed at both stations, is not taken into account by the isotropic k–ε model and therefore a Reynolds stress model may be more appropriate for the calculation of the turbulence levels.

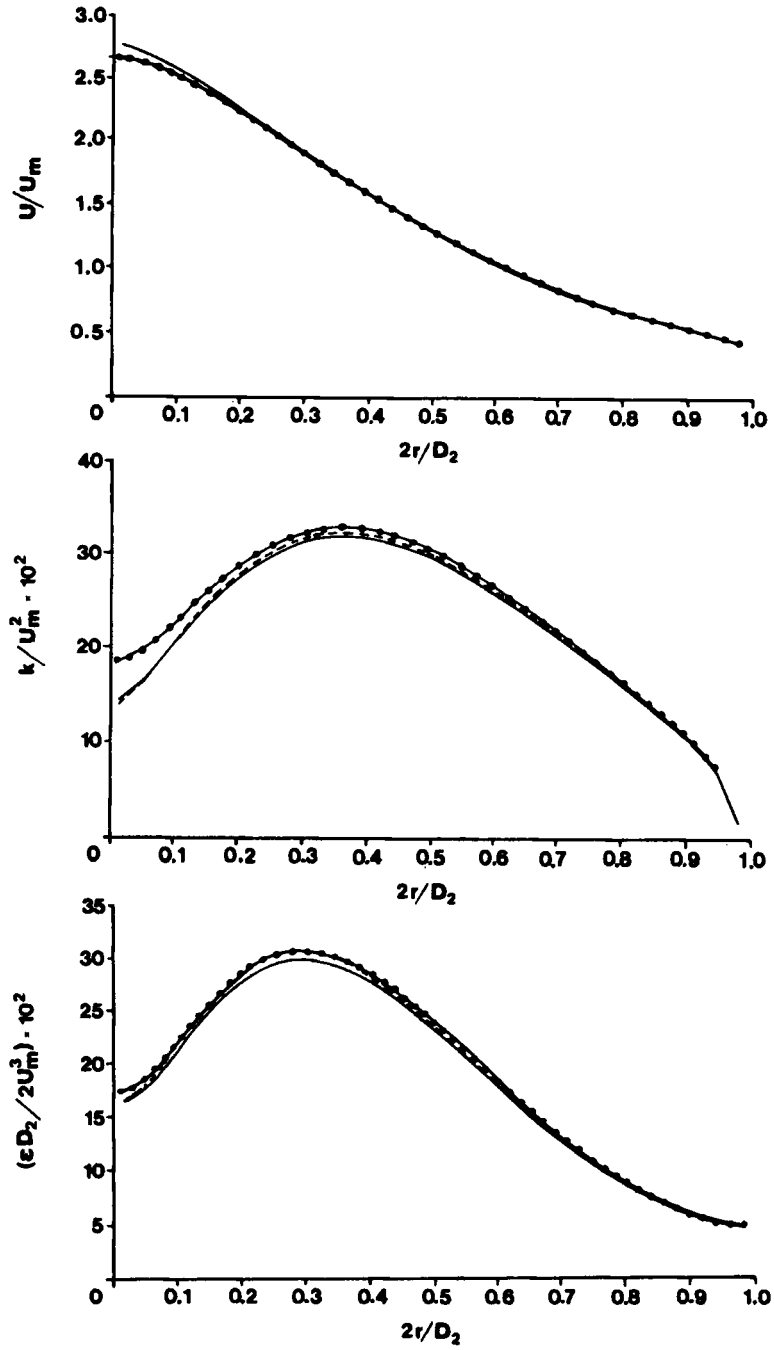

Figure 8. Effect of grid refinement on flow characteristics at first station downstream of diffuser: ——, grid 80 × 30; – – – –, 160 × 30; –●–●–●, 160 × 60.

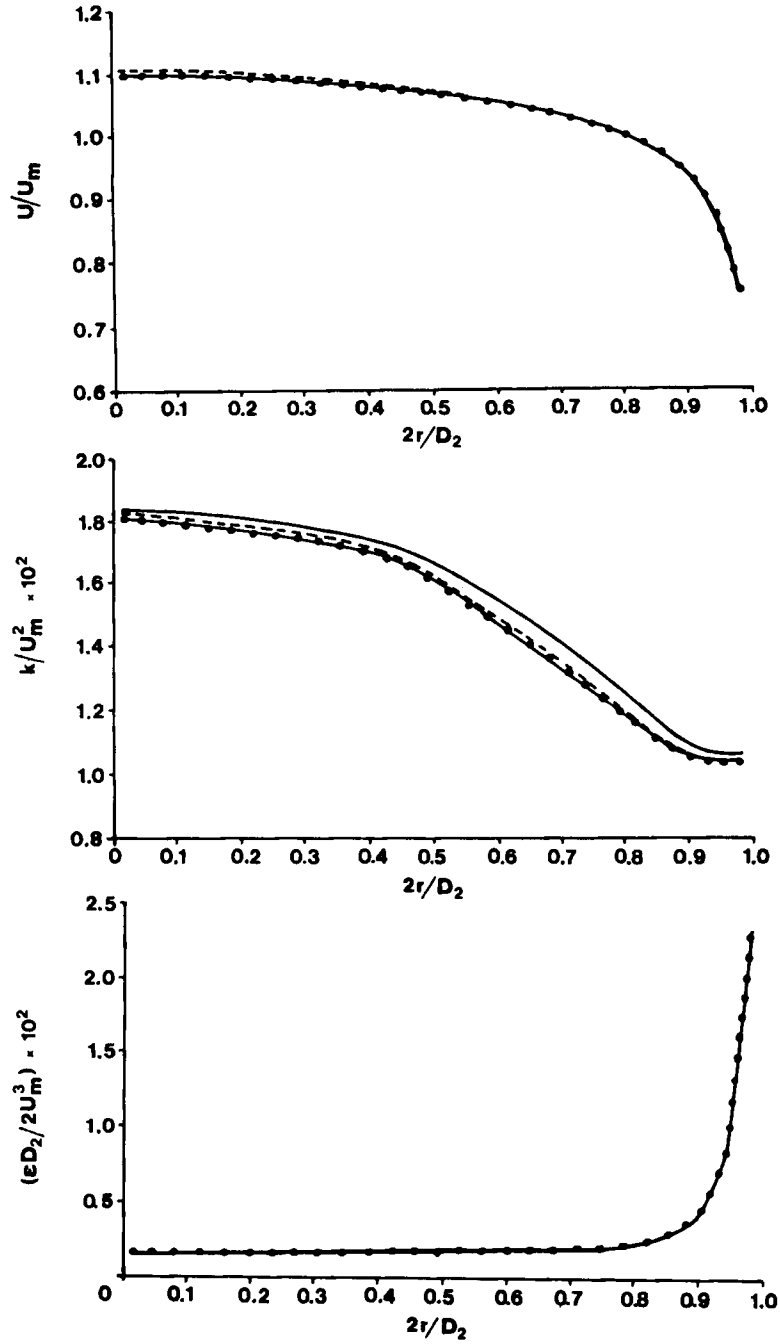

Figure 9. Effect of grid refinement on flow characteristics at second station downstream of diffuser. – – – –, grid 80 × 30; ——, 160 × 30; –●–●–●, 160 × 60

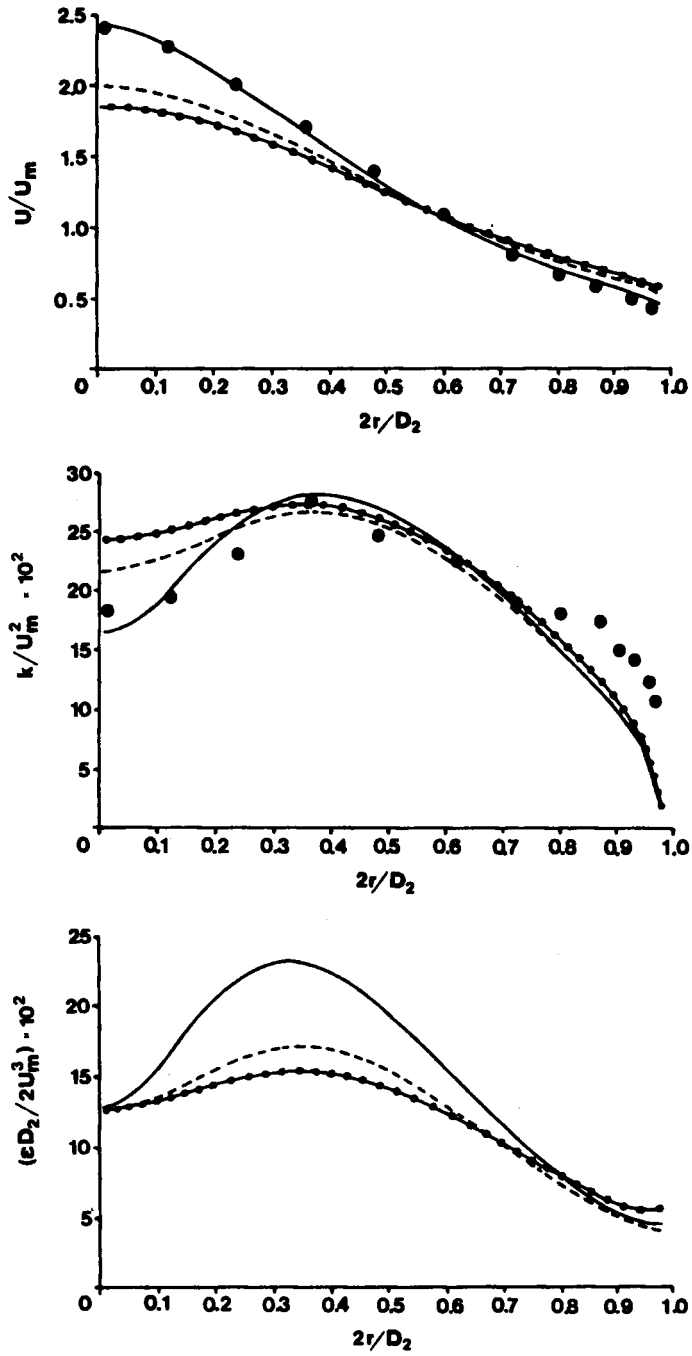

Figure 10. Effect of turbulence model on flow characteristics at first station: ● ● ●, experiments; –●–●–●–, standard k–ε model; ——, modified k–ε ($c_3 = 4{\cdot}44$); – – – –, modified k–ε($c_3 = 2{\cdot}5$)

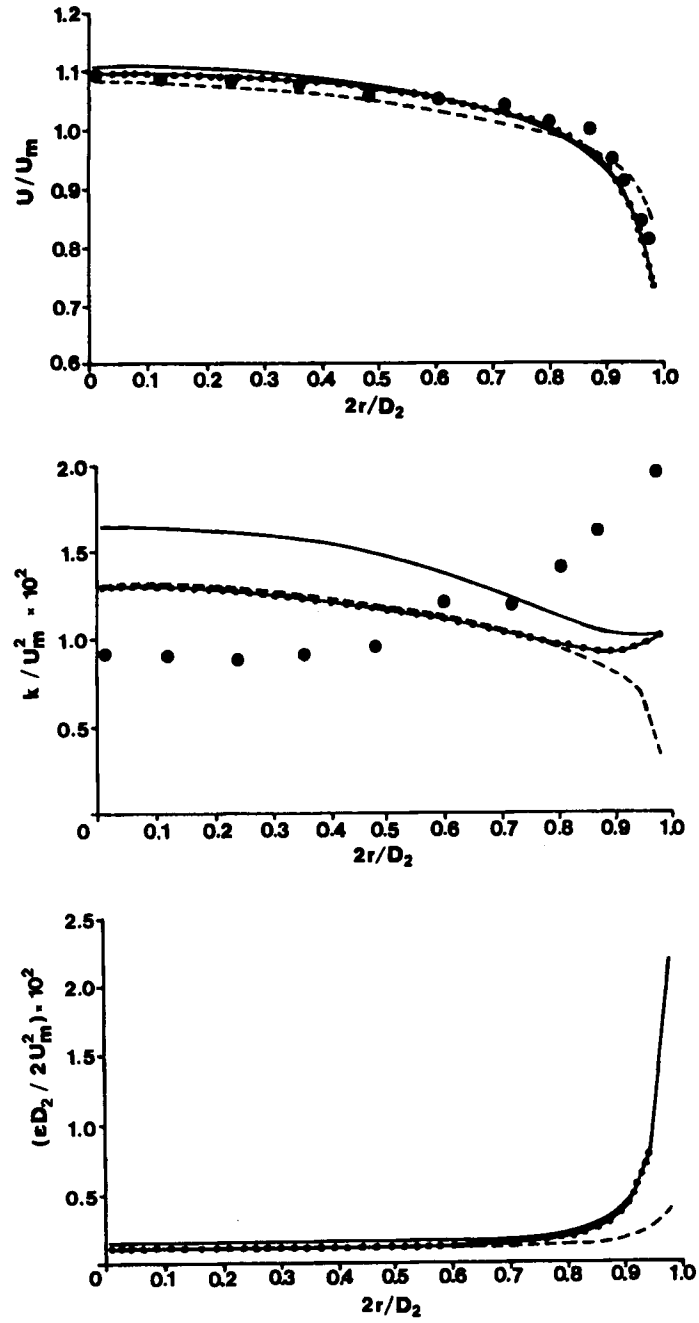

Figure 11. Effect of turbulence model on flow characteristics at second station: ● ● ●, experiments; –●–●–●–, standard k–ε model; ——, modified k–ε($c_3 = 4{\cdot}44$); – – – –, modified k–ε($c_3 = 2{\cdot}5$)

4.3. *Effect of Renolds number*

The effect of Re on the flow characteristics at the two stations was studied by varying the inlet Re from 50 000 to 280 000. Unfortunately, no experimental results were available for other values of Re, except for $Re = 105\,000$. Hence the initial profile used was the fully developed one calculated from a k–ε model for Re 50 000, 105 000 and 280 000. Figures 12(a)–12(c) show the predicted profiles of U, k and ε respectively at the first station using the modified k–ε model ($c_3 = 4{\cdot}44$), since it has been found previously that it performs better in these conditions. Figure 12(a) shows that the flow velocity at this station is influenced by Re. On increasing Re, the velocity profile becomes sharper, indicating the influence of Re on velocity.

Figures 13(a)–13(c) show the respective profiles at the second station, where it is seen that the velocity profile in the region is little affected by Re while the k-profile is affected near the wall.

4.4. *Effect of inlet properties*

The effect of the inlet properties on the flow characteristics was studied by employing the three different profiles described in the previous section at the inlet station of the diffuser. Re was kept equal to 105 000, in line with the experiments.

Figures 14(a)–14(c) show the computed profiles of U, k and ε at the first downstream station using the modified k–ε model. As can be seen the effect of the inlet profile on the flow characteristics is significant. The fully developed profile produces a sharper velocity profile and also increased energy of turbulence at this station. The uniform inlet profile produces a flat part near the symmetry axis and low turbulence levels.

Figures 15(a)–15(c) show the respective profiles at the second downstream station. At this station the inlet profile is shown to affect the characteristics of the flow less, indicating that the flow is redeveloping in this region.

5. CONCLUSIONS

The flow characteristics in the region downstream of a conical diffuser computed by a k–ε model of turbulence are compared with experimental measurements $1D_2$ and $10D_2$ after the diffuser outlet. From the work the following conclusions can be drawn.

(a) A very fine grid is necessary to obtain grid-independent results, especially for the turbulent kinetic energy in regions with high velocity gradients.

(b) The standard k–ε model does not specifically include the effects of adverse pressure on turbulence. As a result it did not perform well even at the mean velocity level. An attempt to incorporate those effects in the form of a correction in the production kinetic energy improved the mean velocity predictions.

Both models, though, failed completely in the prediction of the kinetic energy of turbulence at both stations where comparisons with experimental data were possible. Given the highly anisotropic behaviour of turbulence downstream of a diffuser, the results are not very surprising, but they point out the necessity of using at least Reynolds-stress-type models so that this anisotropy can be tackled.

In short, k–ε or turbulent-viscosity-type turbulence models are not capable of correctly predicting flow conditions dominated by adverse pressure gradients. It is suggested that Reynolds stress models, where flow anisotropy can be resolved, should be used for this type of flow.

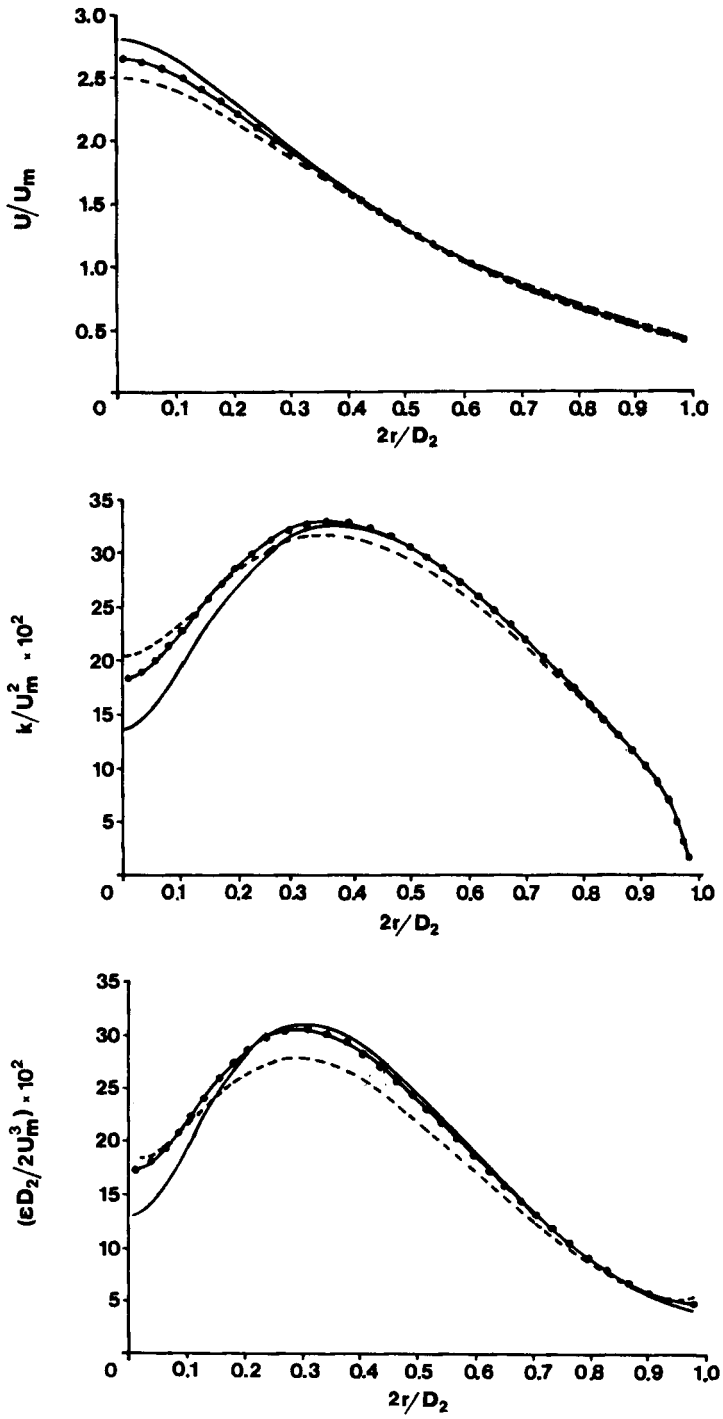

Figure 12. Effect of Reynolds number on flow characteristics at first station: – – – –, $Re = 50\,000$; -●-●-●-, 105 000; — —, 280 000

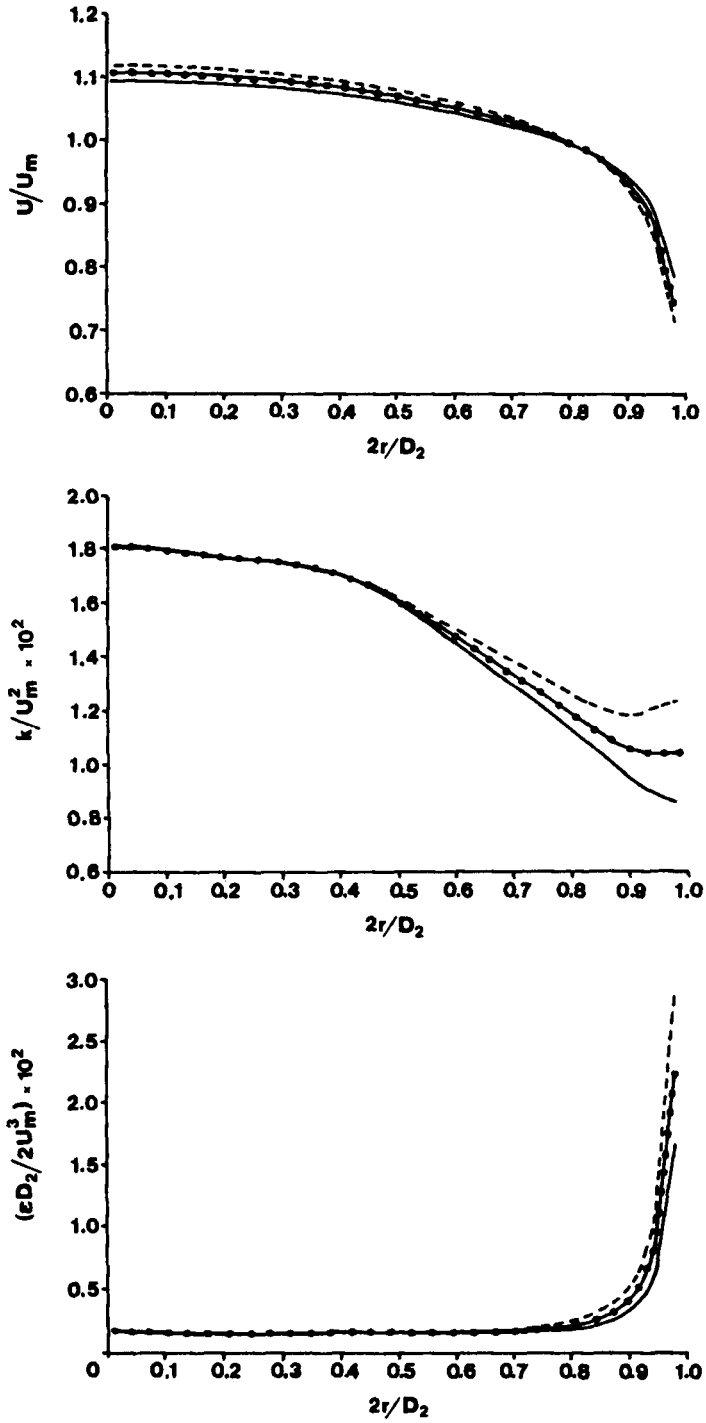

Figure 13. Effect of Reynolds number on flow characteristics at second station: – – – –, $Re = 50\,000$; –●–●–●–, 105 000; ——, 280 000

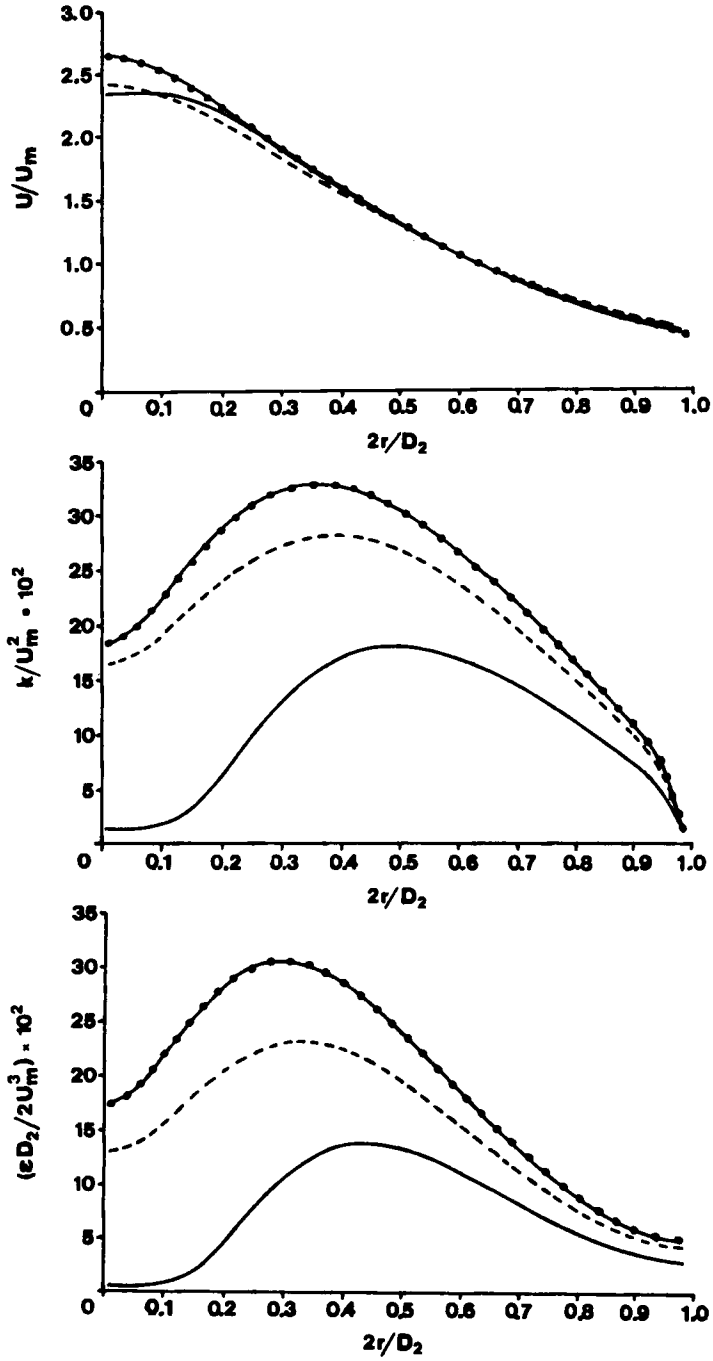

Figure 14. Effect of inlet properties on flow characteristics at first station: ——, uniform; – – – –, experimental; –●–●–●–, fully developed

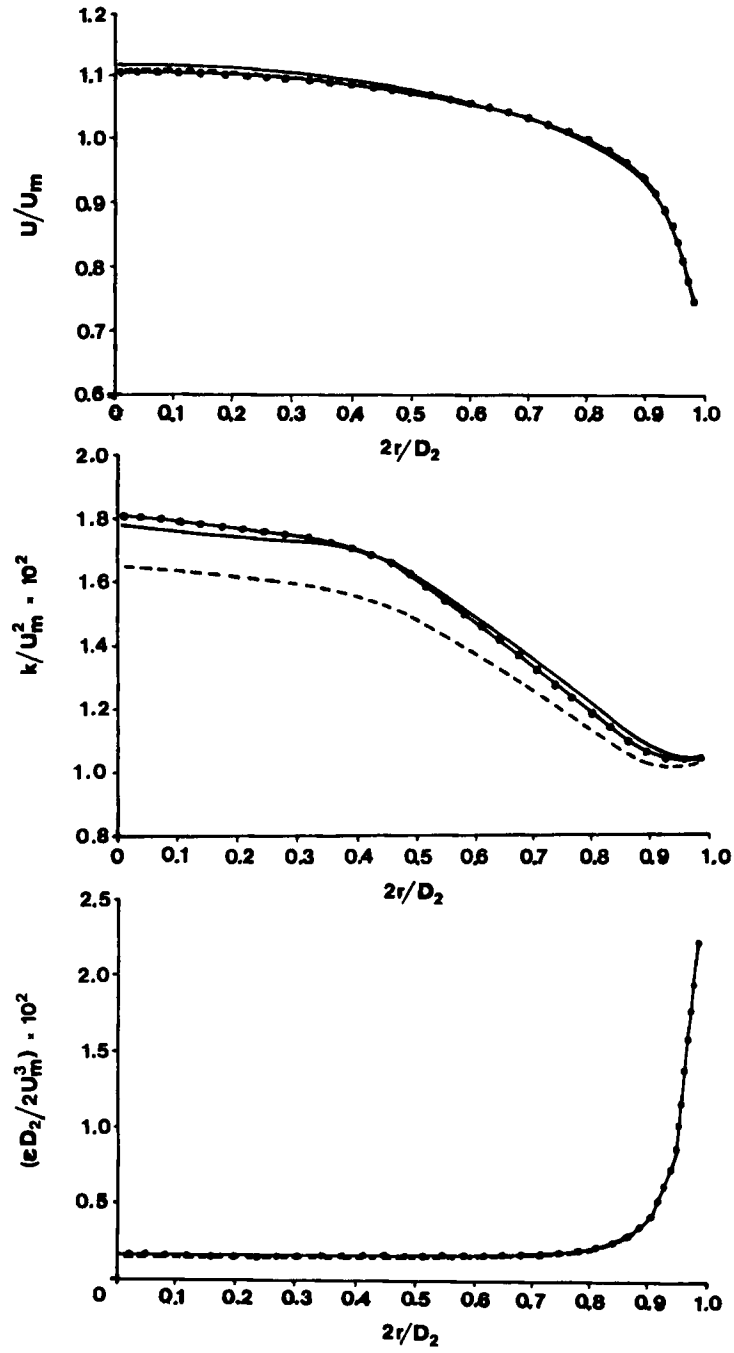

Figure 15. Effect of inlet properties on flow characteristics at second station: ——, uniform; – – – –, experimental; -●-●-●-, fully developed

(c) The effect of the Reynolds number on the flow characteristics is more pronounced at the first downstream station and especially near the symmetry axis.

(d) The effect of the inlet properties on the flow characteristics is very pronounced at the first downstream station, indicating the strong dependence of the turbulence levels on the inlet turbulent kinetic energy. The effect decreases with increasing distance from the inlet.

REFERENCES

1. M. C. Chaturvedi, 'Flow characteristics of axisymmetric expansions', *J. Hydraul. Div., ASCE*, **89**, 61 (1963).
2. N. Weiser and W. Nitsche, 'Experimentelle und numerische Untersuchungen zur algelosten Stromung an einer Rohrstufe mit variablem Offnungswinkel', *ILR-Mitteilung 177*, Institut für Luft-und Raumfahrt, Berlin, 1987.
3. M. Stieglmeier, C. Tropea, N. Weiser and W. Nitsche, 'Experimental investigation of the flow through axisymmetric expansions', *J. Fluids Eng.*, **111**, 464–471 (1989).
4. M. A. Habib and J. H. Whitelaw 'The calculation of turbulent flow in wide-angle diffusers', *Numer. Heat Transfer*, **5**, 145–164 (1982).
5. S. W. Armfield and C. A. Fletcher, 'Numerical simulation of swirling flow in diffusers', *Int. j. numer. methods fluids*, **6**, 541–556 (1986).
6. B. A. Waitman, L. R. Reneau and S. J. Kline, 'Effect of inlet conditions on performance of two-dimensional subsonic diffusers', *J. Basic Eng. D*, **83**, 349 (1961).
7. S. J. Kline, D. F. Abott and R. W. Fix, 'Optimum design of straight walled diffusers', *J. Basic Eng.*, **81**, 321 (1959).
8. J. L. Livesey and J. I. Turner, 'The dependence of diffusers to conditions at their inlet', *J. R. Aeronaut. Soc.*, **69**, 794 (1965).
9. C. I. Bradley and D. J. Cockrell, 'The response of diffusers to conditions at their inlet', *Symp. on Internal Flows*, Univ. of Salford, Salford, 1971, Paper 5, Section A.
10. H. R. Fraser, 'Study of an incompressible turbulent boundary layer in a conical diffuser', *J. Hydraul. Div., ASCE*, **34**, 1–17 (1958).
11. I. Nakamura, K. Ishikawa and Y. Furuya, 'Experiments on the conical diffuser performance with asymmeric uniform shear inlet flow', *Bull. JSME*, **24**, 662–671 (1981).
12. P. A. C. Okwuobi and R. S. Azad, 'Turbulence in a conical diffuser with fully developed flow at entry', *J. Fluid Mech.*, **57**, 603–622 (1973).
13. R. S. Azad and S. Z. Kassab, 'Turbulent flow in a conical diffuser. Overview and implications', *Phys. Fluids A*, **1**, 564–573 (1989).
14. P. Prinos and A. Goulas, 'Flow characteristics downstream of a diffuser', *Proc. XXIV IAHR Congr.*, 1991, C171–C181, Madrid, Spain.
15. V. Christoforou, K. Fotea and A. Goulas, 'Velocity and turbulence measurements in pipe components', *Report prepared for EEC/BCR, TR01/89*, 1989.
16. W. Rodi and G. Scheuerer, 'Scrutinizing the k–ε turbulence model under adverse pressure gradient conditions', *J. Fluids Eng.*, **104**, 174–179 (1982).
17. K. Hanjalic and B. E. Launder, 'Sensitizing the dissipation equation to irrotational strains', *J. Fluids Eng.*, **102**, 34–40 (1980).
18. V. De Henau, G. D. Raithby and B. E. Thompson, 'Prediction of flows with strong curvature and pressure gradient using the k–ε turbulence model', *J. Fluids Eng.*, **112**, 40–47 (1990).
19. Y. Nagano and M. Tagawa, 'An improved k–ε model for boundary layer flows', *J. Fluids Eng.*, **112**, 33–39 (1990).
20. B. E. Launder and D. B. Spalding, 'The numerical computation of turbulent flow', *Comput. Methods appl. Mech. Eng.*, **3**, 269 (1974).
21. S. V. Patankar, 1980. *Numerical Heat Transfer and Fluid Flow*, Hemisphere, New York, 1980.
22. J. F. Thompson, F. C. Thames and C. W. Mastin, 'Boundary fitted curvilinear coordinate system for solution of partial differential equations of fields containing any number of arbitrary two-dimensional bodies', *Rep. GR-2729*, NASA Langley Research Centre, 1976.
23. I. Demirdzic, A. D. Gosman, R. I. Issa and M. Peric 'A calculation procedure for turbulent flow in complex geometries', *Computers and Fluids*, **15**, 251–273 (1987).
24. C. M. Rhie and W. C. Chow, 'Numerical study of the turbulent flow past an airfoil with trailing edge separation', *AIAA J.*, **21**, 1525–1532 (1983).
25. M. Peric, 'A finite volume method for the prediction of three-dimensional fluid flow in complex ducts', *Ph.D. Thesis*, Imperial College, London, 1985.
26. S. Majumdar, 'Development of a finite volume procedure for prediction of fluid flow problems with complex irregular boundaries', *SFB210/T/29*, University of Karlsruhe, 1986.
27. W. Rodi, *Turbulence Models in Hydraulics*, IAHR Publication, 1980.